Entrainment Effect of a Leading-Edge Vortex

N. G. Verhaagen* and A.C.H. Kruisbrink†
Delft University of Technology, Delft, the Netherlands

An investigation into the characteristics of the flow inside a leading-edge vortex is described. The objective of the investigation is to support the development of mathematical models for leading-edge vortex flow by measuring in detail the flow properties of the conical part of a leading-edge vortex, and by comparing these results with theory. The velocity distribution inside the core is well predicted by Stewartson and Hall's outer solution, and the resulting distributions of the entrainment and circulation correlate well with the measured distributions. The effect of the inclusion of the entrainment on the computed characteristics of a slender delta wing is demonstrated using a higher-order panel method.

Nomenclature

a	= slenderness ratio rotational core, $=R/x$
A_{el}	= area of grid element, m^2
$\mathcal{R}$	= aspect ratio
b	= wingspan, m
c_0	= root chord length, m
$C(x,r)$	= circulation, m^2/s
$I(x,r)$	= entrainment, m^2/s
$M(x,r)$	= axial mass flow through rotational core, kg/s
p	= static pressure
p_t	= total pressure
q	= dynamic pressure
$Q(x)$	= sink strength, m^2/s
r	= radial distance to vortex axis, m
R	= radius of rotational core, m
Re	= Reynolds number, $=U_\infty c_0/\nu$
s	= local wing semispan, m
u,v,w	= velocity components parallel and perpendicular to the vortex axis, m/s
u_s,v_s,w_s	= velocity components parallel and perpendicular to freestream, m/s
U	= axial velocity component at the edge of the rotational core, m/s
U_∞	= freestream velocity, m/s
v_r	= radial velocity component, m/s
v_θ	= circumferential velocity component, m/s
V_θ	= circumferential velocity component at the edge of the rotational core, m/s
x,y,z	= coordinates along and perpendicular to the vortex axis, origin in wing apex, m
x_m	= distance from traversing plane to apex, m
x_w,y_w,z_w	= coordinates of wing axes system, origin in wing apex, m
y_m,z_m	= coordinates in traversing plane, m
γ	= semivertex angle, $=\arctan(R/x)$
$\Gamma(x)$	= vortex strength, m^2/s
δ	= $\arctan(r/x)$
θ	= angular coordinate
ν	= kinematic viscosity, m^2/s
ρ	= density, kg/m^3
ω	= vorticity, s^{-1}

Subscripts

el	= grid element
∞	= freestream

Introduction

THIN, slender wings with highly swept and relatively sharp leading edges are employed for several modern aircraft. At moderate and high angles of attack the flow separates at the leading edge, resulting in a steady and stable so-called leading-edge vortex flow.

Experimental investigation by Lambourne and Bryer,[1] Earnshaw,[2] Hummel,[3] Verhaagen,[4] and many others, have helped in obtaining a good insight into the topology of the leading-edge vortex flow and have formed a basis for the derivation of physically correct computational flow models. A recent review of computational methods for vortex flow about slender wings has been given by Hoeijmakers.[5]

Presently, there are two types of computational methods for computing the high-Reynolds-number flow about wings with vortex flow. The first type of method is the free-vortex-sheet method in which the vortex sheets and vortex cores are "fitted" into the potential-flow solution. These methods have demonstrated to produce a reasonable prediction of the wing-surface pressure distribution of slender delta wings.[6-8] The second type of method are those that solve Euler's equations for inviscid rotational flow. Here, the vortex sheets and vortex cores are "captured" automatically in the finite difference/volume solution.

In literature, insufficient experimental data are available to evaluate the computed flow characteristics. The objective of the present investigation is to provide detailed measurements of the flowfield of a leading-edge vortex, thus aiding in the development of improved mathematical flow models. The investigation involved detailed five-hole probe surveys of the vortex flowfield over a large delta-wing half model.

The present paper first gives a description of the physics of leading-edge vortex flow and of existing mathematical models. Theoretical expressions are derived for the entrainment and circulation of a conical core. Subsequently, details and test results of the present wind-tunnel investigation are given and compared with theory. Finally, the effect of the entrainment into the core on the computed chracteristics of a slender delta wing is demonstrated.

Physics of Leading-Edge Vortex Flow

In Fig. 1, the well-known structure of a leading-edge vortex is sketched, as well as the velocity and pressure distribution, along a traverse through the vortex axis (the distributions are diagrammatically reproduced from the present test results). The free shear layer that emanates from the leading edge is

Presented as Paper 85-1584 at the AIAA Fluid Dynamics, Plasmadynamics and Lasers Conference, Cincinnati, OH, July 16-18, 1985; received Oct. 14, 1985; revision received Nov. 18, 1986. Copyright © American Institute of Aeronautics and Astronautics, Inc., 1987. All rights reserved.

*Research Associate, Faculty of Aerospace Engineering.
†Research Engineer; presently, Delft Hydraulics Laboratory, Industrial Hydrodynamics Division.

characterized by a rapid change in the direction of the velocity vector and by a reduction of the total pressure. The latter is caused by the low-energy flow in the shear layer. Through viscous forces, the thickness of the shear layer increases with distance from the leading edge. During the further development of the spiraling shear layer, the distance between the loops becomes of the same order as the thickness of the layer, and a region is formed, called the rotational core, where viscous diffusion has smoothed out completely the gradients in the velocity and pressure distribution. Inside this core, hence, a shear layer can no longer be detected.

Inside the rotational core, the axial and circumferential velocity components increase toward the vortex axis, while the pressure decreases. The circumferential velocity component has its maximum value at the edge of the subcore. Inside this core viscous forces dominate. It is characterized by large gradients of velocity and pressure. As a consequence of the low static pressure at the vortex axis, spiraling flow is sucked into the rotational core and converted there into axial flow. Since the core is permanently fed with vorticity originating at the leading edge, it will grow in size and strength with distance from the wing apex.

Mathematical Modeling

The mathematical model of the leading-edge vortex flow about slender delta wings used in free-vortex-sheet panel methods[6-8] is depicted in Fig. 2. In this high-Reynolds-number model, it is assumed that the boundary layer is very thin and thus can be neglected, while the free shear layer becomes a vortex sheet. In the model, the spiraling free vortex sheet with an infinite number of turns represents the vortex core. To keep computing time within limits, the outer part of the vortex sheet is cut off at a minimum length. The remaining tightly wound inner part of the vortex sheet is used to represent the core. For the computational method, only the effect of the core on the outer potential flow is of interest.

On the free vortex sheet, the vorticity vector is parallel to the mean streamlines. This means that near the leading edge the vorticity vector is almost parallel to the leading edge. Farther downstream, the vector follows the spiraling streamline and eventually will be directed parallel to the vortex axis in the center of the core. The vorticity vector has a component parallel to the vortex axis and two components in the plane perpendicular to the vortex axis, i.e., the circumferential and the radial component. In the computational model for the tightly rolled-up part of the core, the axial-vorticity component is represented by a line vortex located on the vortex axis, the strength of this vortex being equal to the circulation around the core. The radial component is represented by the feeding sheet. The effect of the circumferential vorticity component is like that of ring vortices, i.e., to generate an axial-velocity component inside and a radial component outside the core. The latter one, the entrainment into the core, can be incorporated as a line sink along the vortex axis.

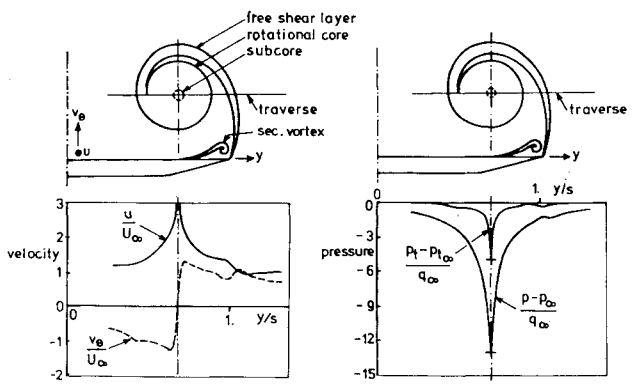

Fig. 1 Traverse of velocity and pressure through the axis of a leading-edge vortex.

In the higher-order panel method of Ref. 7, the strength of the line vortex as well as its position are computed as part of the solution. The sink strength is deduced from the solution for a slender conical vortex core given by Stewartson and Hall.[9] Since the magnitude of the sink strength affects the shape and position of the vortex sheet and vortex core, and hence the computed characteristics of slender delta wings, the present experimental investigation of the vortex core entrainment will aid in improving the mathematical vortex-flow model.

In the other type of computational methods, the Euler codes, the vortex sheets and vortex cores are "captured" as part of the solution, viz., as flow regions with distributed spatial vorticity. The physical relevance of these rotational flow regions, evolving during the time-dependent computational procedure, probably as a result of artificial viscosity effects, at present still is subject to some debate.[5]

Theoretical Relations for the Core

In the following, theoretical relations are derived for the circulation and entrainment of a slender, axisymmetric, conical rotational core. As a basis, the inviscid and incompressible Euler solution for such a core is employed, derived earlier by Stewartson and Hall.[9] The solution reads

$$u/U = 1 - \alpha \ell n(r/R)$$

$$v_\theta/U = \sqrt{(V_\theta/U)^2 - \alpha^2 \ell n(r/R)}$$

$$v_r/U = -\tfrac{1}{2}\alpha a(r/R) \qquad (1)$$

where

$$\alpha = -1 + \sqrt{1 + 2(V_\theta/U)^2} > 0$$

$$a^2 = (R/x)^2 \ll 1$$

r denotes the radius of the core cross section, and u, v_θ, and v_r the axial, circumferential, and radial velocity components,

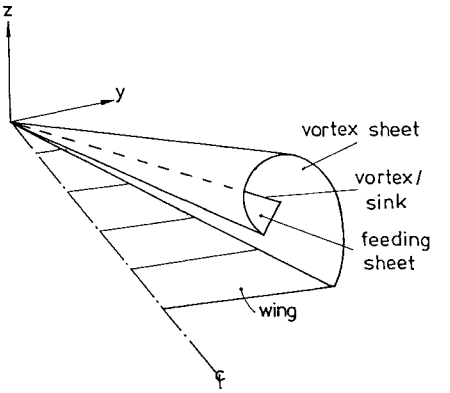

Fig. 2 Model of leading-edge vortex (free-vortex-sheet method).

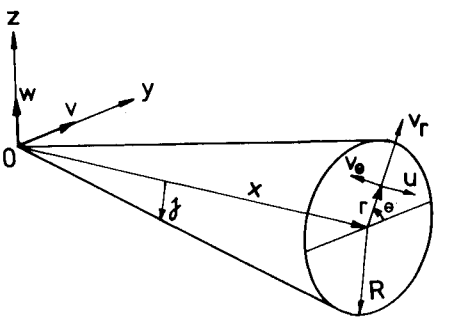

Fig. 3 Model of conical core.

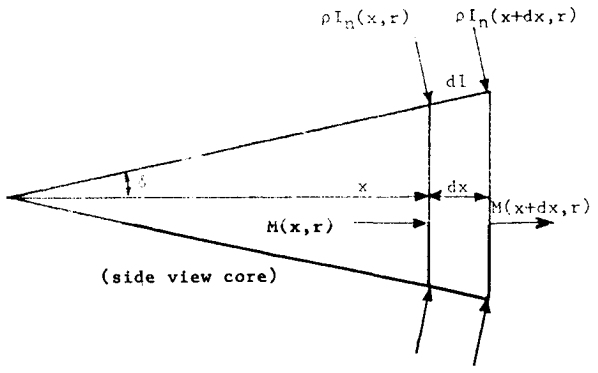

Fig. 4 Mass flow through slice of rotational core.

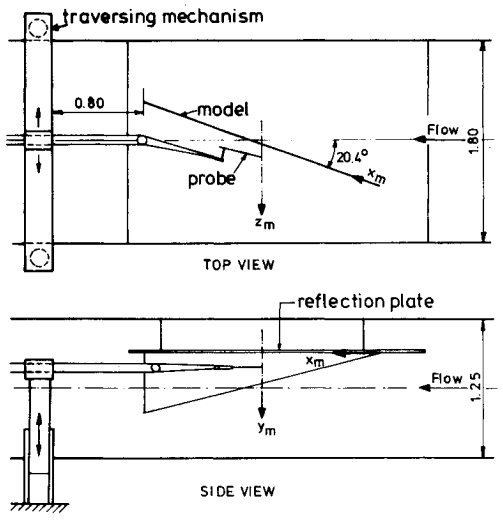

Fig. 5 Experimental test setup (dimensions in m).

respectively (Fig. 3). At the outer edge of the core ($r=R$), a, U, and V_θ are specified constants. The axial and circumferential velocity components have a logarithmic singularity at the axis of the vortex ($r=0$). The radial velocity component has a negative value, suggesting a radial inflow through the envelope of the core. This phenomenon, called entrainment, physically is a consequence of the pressure deficit in the core. For a circular cross section at station x, the circulation can be written as

$$C(x,r)=2\pi r v_\theta \tag{2}$$

With theoretical velocity distribution [Eq. (1)], this yields, in dimensionless form,

$$\frac{C(x,r)}{Ux}=2\pi\left(\frac{r}{x}\right)\sqrt{\left(\frac{V_\theta}{U}\right)^2-\alpha^2\ell n\left(\frac{r}{R}\right)} \tag{3}$$

The vortex strength being equal to the circulation around the rotational core ($r=R$) becomes

$$\Gamma(x)=2\pi R V_\theta \tag{4}$$

The entrainment at station x is equal to the total amount of inflow and can, in general, be expressed as

$$I(x,r)=-\int v\cdot n_c \mathrm{d}s$$

where v is the velocity vector and n_c is the vector normal to the outer edge of the core cross section. In the present case of the slender axisymmetric conical core, the entrainment becomes

$$I(x,r)=-2\pi r v_r \tag{5}$$

With Eq. (1) this yields, in dimensionless form,

$$\frac{I(x,r)}{Ux}=\pi\left(\frac{r}{x}\right)^2\alpha \tag{6}$$

This expression indicates that the entrainment increases with radial distance from the vortex axis. This is due to the fact that the amount of circumferential vorticity inside the contour increases as well.

For the present experimental investigation, the measurement accuracy of the axial velocity component was found to be higher than that of the radial component. Since the radial inflow across the core will increase the axial mass flow through the core cross section (mass conservation law), the entrainment can also be determined from the rate of change with x of the axial mass flow. Consider a slice of thickness dx (Fig. 4). The axial mass flow at station x through a cross section with radius r can be written as

$$M(x,r)=\rho\int_{\theta=0}^{2\pi}\int_{\eta=0}^{r} u\eta \mathrm{d}\eta\mathrm{d}\theta$$

while the local inflow through the envelope of the core is given by

$$I_n(x,r)=-r\int v\cdot n\mathrm{d}\theta \tag{7}$$

where n is the vector normal to the envelope. This inflow is a consequence of the axial inflow, which crosses the envelope due to the increment of its cross section with x and of the radial inflow into the core. Equation (7) thus can be expressed as

$$I_n(x,r)=2\pi r(-v_r\cos\delta+u\sin\delta) \tag{8}$$

where $\delta=\arctan(r/x)$.

Conservation of mass yields (Fig. 4):

$$M(x+\mathrm{d}x,r)=M(x,r)+\tfrac{1}{2}\rho[I_n(x,r)+I_n(x+\mathrm{d}x,r)]\mathrm{d}l \tag{9}$$

Due to conicity, the axial mass flow can be written as

$$M(x,r)=\frac{\rho x}{2\cos\delta}I_n(x,r)$$

With Eq. (8), this becomes

$$M(x,r)=\frac{\rho x}{2}\left[-2\pi r v_r+2\pi r u\left(\frac{r}{x}\right)\right]$$

Substituting Eq. (5), the following dimensionless expression can be formulated:

$$\frac{I(x,r)}{Ux}=\frac{2}{\rho}\frac{M(x,r)}{Ux^2}-2\pi\left(\frac{r}{x}\right)^2\frac{u}{U} \tag{10}$$

With this expression, the entrainment can be determined from the axial velocity distribution at a station x. Substituting of the theoretical velocity distribution given by Eq. (1) yields an expression identical to Eq. (5).

The sink strength of the core required in the computational model is equal to the entrainment into the rotational core ($r=R$) and can be expressed as

$$Q(x)=-2\pi R V_r$$

Using Eq. (1), this can also be written as

$$\frac{Q(x)}{Ux} = \pi a^2[-1+\sqrt{1+2(V_\theta/U)^2}] \tag{11}$$

This form illustrates that, at least for the slender conical core, the sink strength depends on the swirl ratio V_θ/U.

It should be remarked here that the expressions used in this section for the entrainment and the sink strength are different from the expressions used in an earlier publication.[10]

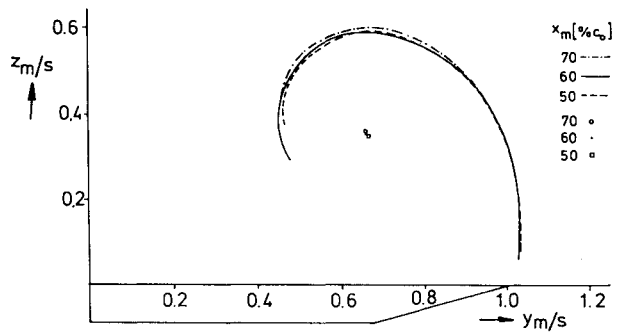

Fig. 6 Position of shear layer and vortex axis for the three traversing planes.

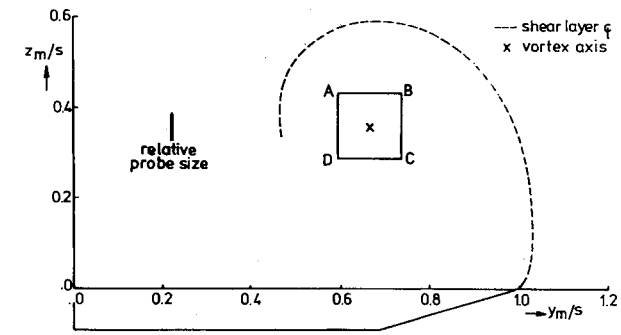

Fig. 7 Contour of core grid and probe size, traversing plane of 50% c_0.

Experimental Setup

Wind Tunnel and Test Conditions

The investigation was carried out in the low-speed wind tunnel of the Technical University Delft (TUD) Department of Aerospace Engineering. The wind tunnel has an octagonal test section 1.25 m high × 1.80 m wide, and a turbulence level of about 0.05% at the speed of 25 m/s used in the present investigation. The Reynolds number was 3.8×10^6, based on model root chord length.

Model

As vortex generator, a large half-model of a unit-aspect-ratio sharp-edged delta wing was used mounted vertically from a reflection plate at the top of the test section (Fig. 5). The flat-plate Duraluminium model has 0.3-mm-thick leading and trailing edges. In order to have the leeward side flat, these edges were chamfered on the windward side only. The model has a root chord length of 2.22 m, a thickness of 25 mm, and a fixed geometric angle of attack of 20.4 deg.

Probes

The total-pressure and velocity distribution of the leading-edge vortex were measured with a non-nulling five-hole probe. The probe has an o.d. of 1.65 mm and a clipped conical nose whose semivertex angle is 45 deg. Since the probe is used as non-nulling, probe calibration is necessary. This was carried out in a uniform parallel freestream for flow angles up to 45 deg.

Freestream pressures were measured by a pitot-static probe installed upstream of the vortex generator on the centerline of the test section floor.

The pressure ducts of the five-hole probe and the pitot-static probe were connected to a scanivalve. As reference pressure for the scanivalve, the freestream total pressure was used. The pressure differences were recorded by a minature transducer in conjunction with a electronic pressure indicator. To minimize pressure lag, the scanivalve and transducer were installed close to the probe, viz., inside the forward part of the probe-carrying sting of the traversing mechanism (Fig. 5).

Experimental errors are due to inaccuracies in the probe calibration, alignment, and positioning, as well as the pressure measurements. It is estimated that these inaccuracies result in total pressures accurate within 15% of the freestream total

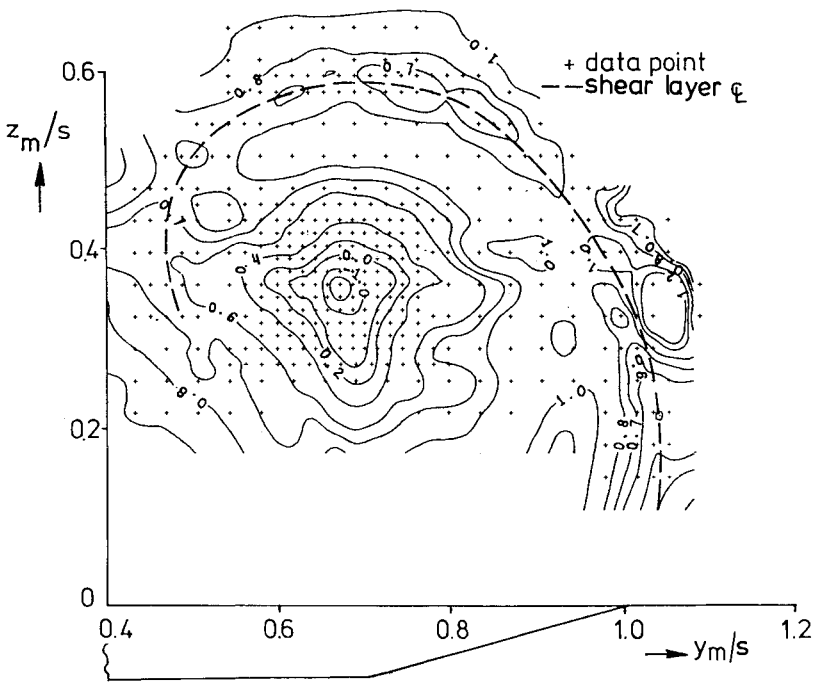

Fig. 8 Contours of constant $(p_t - p_\infty)/q_\infty$.

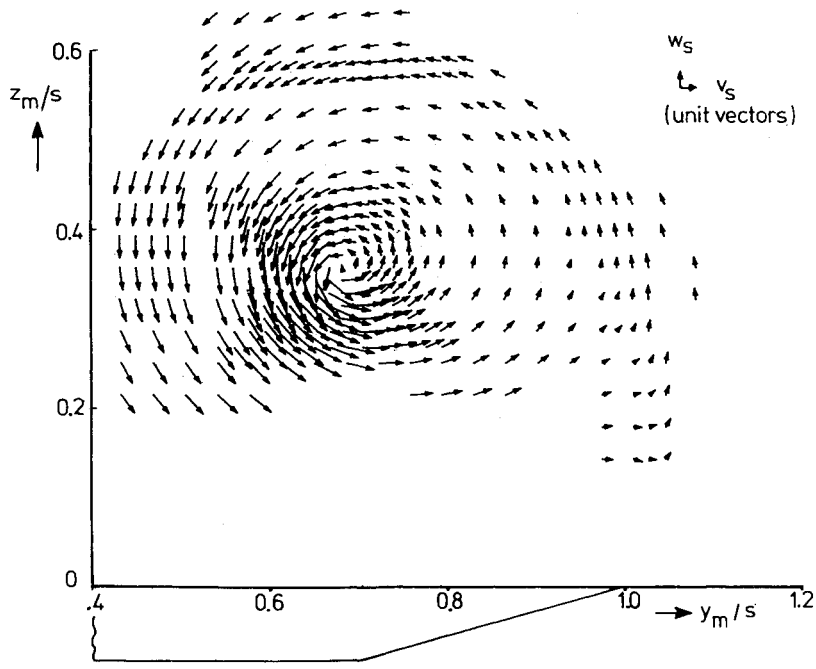

a) Velocity vectors in traversing plane.

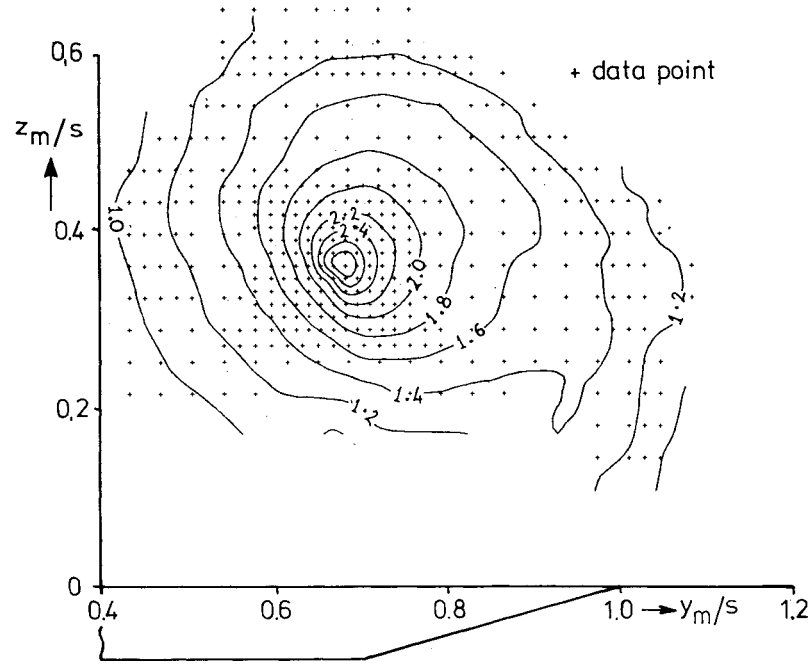

b) Contours of constant u_s/U_∞.

Fig. 9 Velocity distribution in traversing plane of 50% c_0.

pressure, and velocity components accurate within 5% of the freestream velocity.

In regions with high gradients, e.g., the subcore and the free shear layer, the flow differs considerably from the uniform parallel flow condition used for the calibration. It can, therefore, be imagined that the five-hole probe pressures should be corrected for strong three-dimensional gradient effects. Since, to the authors' knowledge, a proven method to calculate these effects is not available, the present measurements were not corrected in this respect.

Data registration and reduction was made using a minicomputer. Flow properties were plotted on line and monitored as the measurements progressed.

Flowfield Surveys

To survey the vortex flowfield, a rigid probe-carrying traversing mechanism installed in the diffusor of the wind tunnel was used (Fig. 5). The surveys were carried out in three traversing planes, each perpendicular to the tunnel axis and intersecting the model at 50, 60, and 70% c_0, respectively. During the test, the attitude of the probe remained fixed. In order to avoid flow angles larger than those for which the probe was calibrated, the probe was more or less aligned with the vortex axis.

Test Results

Conicity of Vortex Flow

The theoretical expressions derived previously for the circulation and entrainment hold for the case of a conical core only. To check the conicity of the leading-edge vortex flow in the three traversing planes, the following was traced:

1) The vortex center, defined as the region where the total pressure has its lowest value.

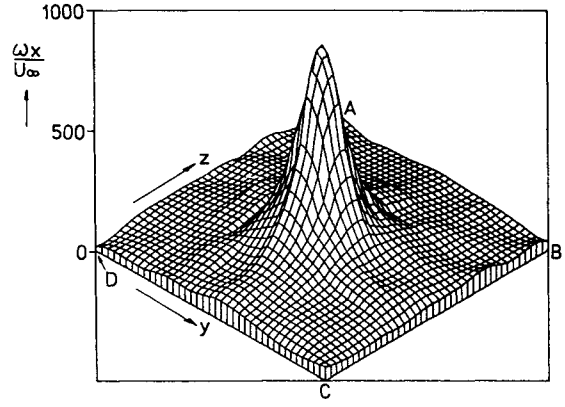

a) Three-dimensional presentation.

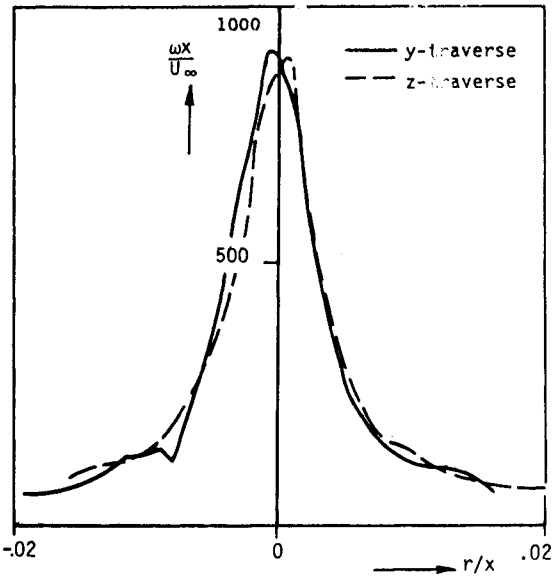

b) y and z traverse through vortex axis.

Fig. 10 Axial vorticity distribution inside region ABCD, cross-flow plane 50% c_0.

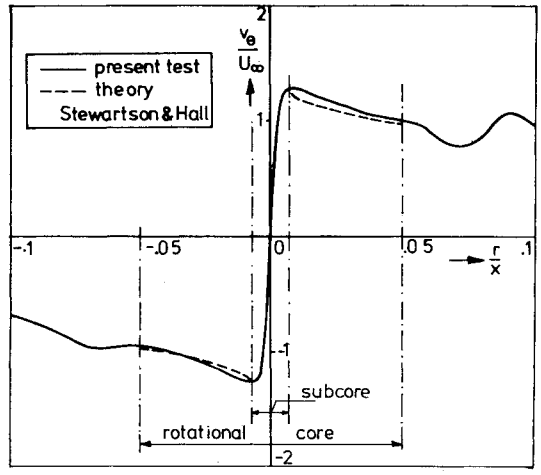

a) Circumferential velocity.

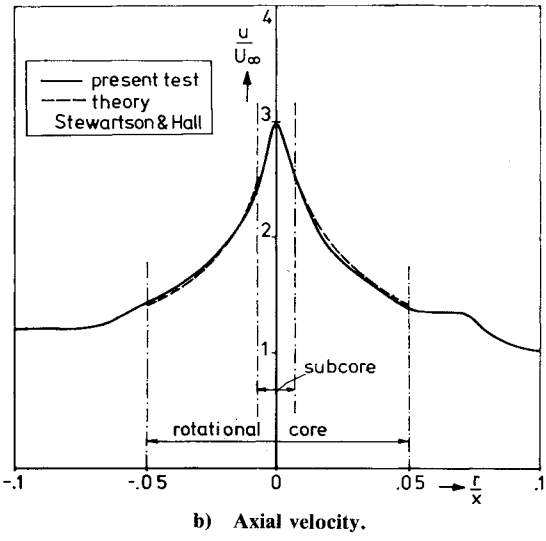

b) Axial velocity.

Fig. 11 Velocity distribution for a y traverse through the vortex axis, cross-flow plane 50% c_0.

2) The centerline of the free shear layer, defined as the curve through the relative minima of the total pressure.

Results are given in Fig. 6 as a function of dimensionless coordinates. For the three planes the differences are small, indicating that it is justified to assume a conical vortex flow up to at least 70% c_0. The slight inboard and upward displacement of the vortex may be due to trailing-edge effects and for the present relatively large model also due to tunnel-wall interference.

An oil-flow investigation of the boundary layer on the leeward side of the model showed a straight secondary-separation line over the greatest part of the wing. The location of the secondary-separation line depends on the status of the boundary layer, in particular, underneath the vortex core. On a flat-plate delta wing at 20-deg incidence, a laminar boundary layer separates at about 65% semispan, while a turbulent boundary layer separates more outboard, viz., at about 90% semispan.[4] On the present model, secondary separation occurs at 90–95% semispan, indicating that the boundary layer is turbulent underneath the core.

The conicity of the velocity field will be addressed subsequently.

Flow Survey at 50% c_0

Pressure and velocity components were measured at points indicated in Figs. 8 and 9. In regions where large gradients could be expected, such as the center of the core and the free shear layer, denser data point grids were selected. As depicted in Fig. 7, the contour of the grid at the core center is marked ABCD. This figure also shows the relative size of the five-hole probe.

Figure 8 shows the contours of the constant total pressure coefficient. The centerline of the shear layer, drawn through the relative minima of the total pressure distribution, could be traced over about a three-quarter turn. At the center of the vortex, the total pressure losses are largest due to accumulated viscous losses. The total pressure coefficient has an absolute minimum value of -3.8 at the vortex axis.

The distribution of the velocity vectors is shown in Fig. 9. Note that since the traversing plane is oblique with respect to the vortex axis, the velocity distributions appear slightly nonaxisymmetric. The velocity vectors in the traversing plane (Fig. 9a) clearly show the direction of rotation of the vortex flow. The magnitude of the velocity vector that is parallel to the tunnel axis increases toward the center of the vortex (Fig. 9b). In this region, values were recorded of up to three times the freestream velocity.

Conicity of Velocity Field

The conicity of the velocity field, one of assumptions underlying the solution of Stewartson and Hall,[9] was investigated by comparing the velocity components inside grid

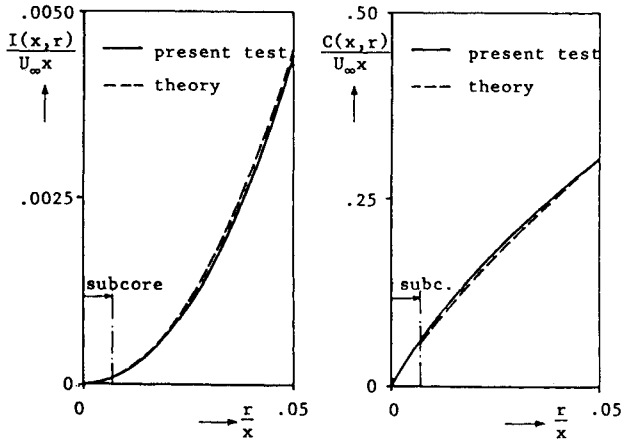

Fig. 12 Distribution of entrainment and circulation inside rotational core.

ABCD in the three traversing planes. Data points in the three planes having identical y_m/s and z_m/s coordinates were situated on one and the same ray through the apex. The investigation showed that from 50 to 70% c_0, the changes of the velocity components are small and of the same order as the estimated accuracy of the measurements. Therefore, it is concluded that, for the present case, the assumption of a conical velocity field is valid indeed. There is one exception; along the vortex axis a slight increase in axial velocity is recorded. This was also noted in Refs. 1 and 2.

Axial Vorticity Distribution

In order to obtain an insight into the axial vorticity distribution at the vortex center (region ABCD), the velocity distribution was determined in the cross-flow plane of 50% c_0. This plane is perpendicular to the vortex axis and passes through $x_m = 50\%\ c_0$ on the root chord. The velocity components at points of the cross-flow plane were calculated from the corresponding points in the three traversing planes by a quadratic interpolation along rays through the apex. In order to obtain a realistic nonlinear velocity distribution, each element was subdivided into 16 smaller ones. Starting from the velocity components of the original elements, those of the smaller ones were calculated by quadratic interpolation. For each small element, the circulation Γ_{el} was calculated by integrating the cross-flow velocity along the edge of the element. The circulation was assigned to the centroid of the element. The vorticity in an element is related to the circulation following the Stokes' theorem:

$$\iint \omega \cdot n \mathrm{d}A_{el} = \int v_t \cdot \mathrm{d}s = \Gamma_{el}$$

The local axial vorticity component is then obtained with

$$\omega_x = \Gamma_{el}/A_{el}$$

The three-dimensional axial vorticity distribution inside ABCD is shown in Fig. 10a. It is characterized by a peak of high vorticity near the vortex axis. This is also evident from Fig. 10b, which depicts the distribution for a y and z traverse through the vortex axis plotted vs dimensionless radial distance r/x. The sign of the latter has been taken positive in the direction of either the positive y axis or positive z axis.

Velocity Distribution Rotational Core

Figure 11 shows the measured distribution of the circumferential and axial velocity in the cross-flow plane of 50% c_0 for a y traverse through the vortex axis. The distributions are plotted vs radial distance r, which, in view of the conicity of the vortex flow, has been made dimensionless with the distance from the apex x. The gradients at $|r/x| > 0.05$ are caused by the free shear layer. The rotational core is a region of continuously distributed rotational flow inside which no shear layer can be detected. For the present case, the radius r/x of the rotational core has been chosen to be 0.05 ($= 20\%\ s$).

The subcore, defined as the region between the maximum values of the circumferential velocity, has a radius r/x of about 0.007 ($\approx 3\%\ s$). In addition to the y traverse, a z traverse was made through the vortex axis. Inside the rotational core, the velocity distribution is quite identical to that presented here for the y traverse, indicating that the flow inside the core is axially symmetric.

Figure 11 also gives the theoretical velocity distribution, which follows from Eq. (1). In this equation, which needs experimental values to generate the velocity distribution, for a, U/U_∞, and V_θ/U the average values measured at the outer edge of the rotational core were substituted. It should be remembered here that the theoretical solution holds only for the annulus between the subcore and the outer edge of the rotational core. As can be seen from the figure, inside this annulus there is a good agreement between the theoretical and experimental velocity distribution. Reference 9 also derives an inner solution for the rotational core giving the velocity distribution inside the viscous subcore. Since for the present investigation only the influence of the core on the outer (potential) flow is of interest, this solution is not considered further here.

Distribution of Entrainment and Circulation

From the experimental velocity distribution inside the rotational core, the distribution of the circulation and the entrainment was calculated using Eqs. (2) and (10). For this calculation, the velocity distribution inside the core was assumed to be axisymmetric. The dimensionless results are presented in Fig. 12. This figure also presents the theoretical distribution of the circulation and the entrainment which results from a velocity distribution as given by Eq. (1). The theoretical distributions were calculated using Eqs. (3) and (6), while for a, U/U_∞, and V_θ/U the values were substituted measured at the edge of the rotational core. As can be noted from the figure, the theoretical distribution of the entrainment and circulation correlate well with the experimental distributions. This also means that the expression of Eq. (11) will yield a valid prediction for the sink strength of the rotational core.

Effect of the Entrainment on Computed Characteristics

With Eq. (4) substituted into Eq. (11), the sink strength can be expressed as

$$\frac{Q(x)}{Ux} = \pi a^2 \left[-1 + \sqrt{1 + 2\left\{ \frac{\Gamma(x)}{2\pi RU} \right\}^2} \right] \tag{12}$$

This yields a relation for the sink strength of the core in terms of its radius and circulation. Equation (12) has been included as an additional equation in the higher-order panel method for the slender-body approximation of the potential flow about slender configurations with leading-edge vortex sheets (VORSBA, a further development of the VORCON code of Ref. 7). The length of the feeding sheet is taken equal to the radius R of the core, while consistent with the approximations involved in the computational model the velocity at the edge of the core U is replaced by the magnitude U_∞ of the freestream velocity. Figure 13 shows numerical results obtained for the present unit-aspect-ratio wind-tunnel model at 20-deg angle of attack. The thickness of the wing has been neglected. The geometry of the vortex sheet and the position of vortex axis are shown in Fig. 13a. The results were obtained for a sheet length of 1.25 times the local semispan, a sheet length often used in free-vortex-sheet methods. Inclusion of

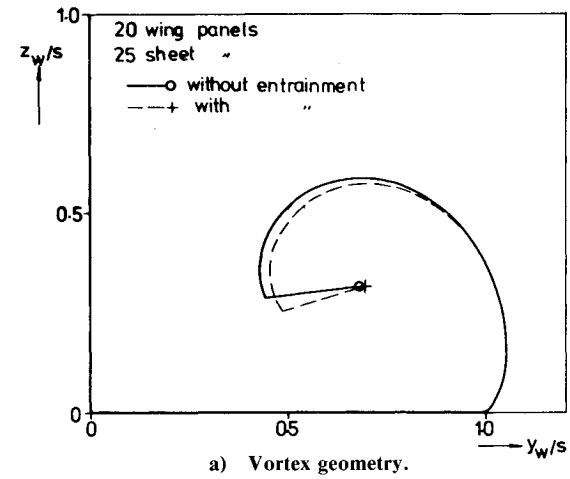

a) Vortex geometry.

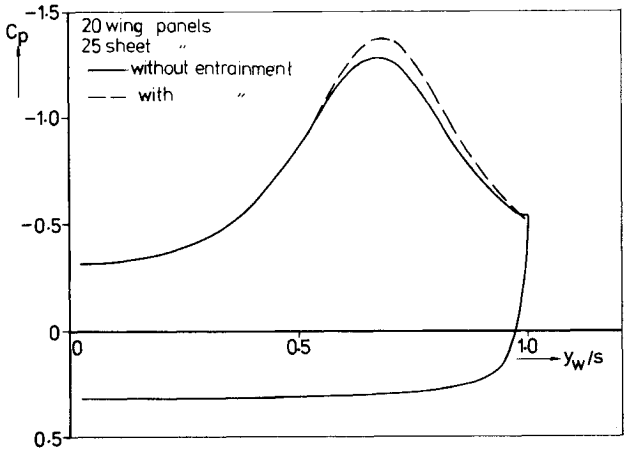

b) Wing-surface pressure distribution.

Fig. 13 Computed results of unit-aspect-ratio delta wing, $\alpha = 20$ deg; conical-flow solution with/without entrainment.

entrainment results in a vortex sheet more circular in appearance and an outboard displacement of the vortex center. Figure 13b shows the effect of the entrainment on the computed wing-surface pressure distribution, indicating that the entrainment increases the suction at the upper wing. This is also reflected in the normal-force coefficient, which is 1.00 for the case without and 1.03 for the case with entrainment included.

Concluding Remarks

Using a small, five-hole probe, the velocity and pressure distribution of the conical part of a large leading-edge vortex was measured in detail. From the measured velocity distribution, the distribution of the axial vorticity component, the circulation, and the entrainment was determined.

The velocity distribution predicted by the Stewartson-Hall Euler solution for an isolated axisymmetric conical vortex core, and the resulting circulation and entrainment correlate well with distributions measured in the present investigation.

In the free-vortex-sheet potential-flow model, the effect of the entrainment can be simulated by a sink distribution along the vortex axis. For the limiting case of conical flow, the effect of including the entrainment is demonstrated using a higher-order panel method.

The present investigation has been carried out for one flow condition and in the conical part of the vortex flow only. Since certainly the incidence and probably to a lesser extent the Reynolds number are expected to be parameters of the entrainment, further investigation is required at other flow conditions and also in the nonconical part of the vortex.

In order to eliminate possible measurement inaccuracies due to probe/vortex-flow interference effects, laser Doppler velocimeter measurements will be included in future investigations.

Acknowledgments

The authors are indebted to J.H.B. Smith of RAE, Farnborough, for his suggestions made to improve the theoretical relations for the entrainment. The authors also wish to express gratitude to Prof. J. L. van Ingen of TUD and to H. W. M. Hoeijmakers of NLR for the valuable discussions. NLR is also gratefully acknowledged for providing the computation results plotted in Fig. 13. The authors are further indebted to H. J. Morre and L. Molenwijk for their assistance in the design and operation of the five-hole probe, the traversing mechanism, and the pressure recording system.

References

[1]Lambourne, N. C. and Bryer, D. W., "Some Measurements in the Vortex Flow Generated by a Sharp Leading Edge Having 65 deg Sweep," ARC CP 477, 1960.

[2]Earnshaw, P. B., "An Experimental Investigation of the Structure of a Leading-Edge Vortex," ARC R&M 3281, 1961.

[3]Hummel, D., "On the Vortex Formation Over a Slender Wing at Large Angle of Incidence," AGARD-CP-247, Paper 14, 1979.

[4]Verhaagen, N. G., "An Experimental Investigation of the Vortex Flow Over Delta and Double-Delta Wings at Low Speed," Dept. of Aerospace Engineering, Delft Univ. of Technology, Rept. LR-372, 1983; also, AGARD-CP-342, Paper 7, 1983.

[5]Hoeijmakers, H.W.M., "Numerical Computation of Vortical Flow About Wings," AGARD Lecture Series Computational Fluid Dynamics, VKI, also, NLR MP 83073 U; March 1984.

[6]Hoeijmakers, H.W.M. and Bennekers, B., "A Computational Method for the Calculation of the Flow About Wings with Leading-Edge Vortices," AGARD-CP-247, Paper 25, 1979.

[7]Hoeijmakers, H.W.M. and Vaatstra, W., "A Higher-Order Panel Method for the Computation of the Flow About Delta Wings with Leading-Edge Separation," NLR MP 81053 U, 1981.

[8]Johnson, F. T., Tinoco, E.N., Lu, P., and Epton, M.A., "Three-Dimensional Flow Over Wings with Leading-Edge Vortex Separation," *AIAA Journal*, Vol. 18, April 1980, pp. 367–380.

[9]Stewartson, K. and Hall, M. G., "The Inner Viscous Solution for the Core of a Leading-Edge Vortex," *Journal of Fluid Mechanics*, Vol. 15, 1963, pp. 306–138.

[10]Verhaagen, N. G. and Van der Snoek, L., "An Experimental Investigation of the Entrainment into a Leading-Edge Vortex," Dept. of Aerospace Engineering, Delft Univ. of Technology, the Netherlands, Rept. LR-332, 1981.